PROTEINS
STRUCTURE ■ FUNCTION ■ BIOINFORMATICS

Spontaneous β-barrel formation: An all-atom Monte Carlo study of $A\beta_{16-22}$ oligomerization

Anders Irbäck* and Simon Mitternacht

Computational Biology and Biological Physics Group, Department of Theoretical Physics, Lund University, SE-223 62 Lund, Sweden

ABSTRACT

Using all-atom Monte Carlo simulations with implicit water, combined with a cluster size analysis, we study the aggregation of $A\beta_{16-22}$, a peptide capable of forming amyloid fibrils. We consider a system of six initially randomly oriented $A\beta_{16-22}$ peptides, and investigate the thermodynamics and structural properties of aggregates formed by this system. The system is unaggregated without ordered secondary structure at high temperature, and forms β-sheet rich aggregates at low temperature. At the crossover between these two regimes, we find that clusters of all sizes occur, whereas the β-strand content is low. In one of several runs, we observe the spontaneous formation of a β-barrel with six antiparallel strands. The β-barrel stands out as the by far most long-lived aggregate seen in our simulations.

Proteins 2008; 71:207–214.

Key words: protein aggregation; protein misfolding; self-assembly; amyloid-β; cluster size analysis.

INTRODUCTION

Amyloid fibril formation is a symptom of several human neurodegenerative diseases, but increasing evidence suggests that the neurotoxic agent is not the fibrils themselves.[1] Much current research is directed at characterizing small soluble oligomers of amyloid proteins, in order to identify the major toxic species.[2] For example, in a study of Alzheimer's amyloid-β protein, Aβ, it was found that 56-kDa Aβ assemblies could be linked to loss of memory function in mouse and rat.[3]

While atomic-level structural models have now emerged for some amyloid fibrils,[4–7] less is known about the detailed structure of the oligomeric states. These states are difficult to characterize because of their transient nature—they can transform into other classes of oligomers, break up into monomers, or move onto fibril formation (which is probably an irreversible process so that there is no equilibrium distribution). On the other hand, there are some common classes of oligomeric states that have been observed for several amyloid proteins such as spherical, chain-like, and annular species.[8] One possible explanation of neurotoxicity is that annular pore-like aggregates cause membrane permeabilization.[8,9]

Here, we explore the structure and stability of small $A\beta_{16-22}$ oligomers by all-atom Monte Carlo (MC) simulations for a system of six $A\beta_{16-22}$ peptides. This seven-residue fragment of Aβ is known to be able to make amyloid fibrils.[10] Furthermore, it has been demonstrated, by solid-state NMR, that the β-strand organization is antiparallel in $A\beta_{16-22}$ fibrils.[10,11] A recent study of $A\beta_{16-22}$ by infrared spectroscopy (IR) found evidence for antiparallel β-sheet structure also in solution.[12]

The availability of experimental data, its small size, and the fact that it spans an aggregation-prone region of Aβ,[13] make the $A\beta_{16-22}$ peptide a suitable model system for computational studies, and simulations of $A\beta_{16-22}$ aggregation have been reported by several groups.[14–23] Here, we study $A\beta_{16-22}$ oligomerization by unbiased thermodynamic simulations started from random initial conformations. We use a simple but novel procedure to identify which clusters are formed in a given multichain conformation. Another novelty is that we observe the spontaneous formation of a β-barrel. The formation of annular, β-barrel-like structures[24,25] and open high-curvature β-sheets[26,27] has previously been seen in simulations based on coarse-grained models, but as far as we know, not in atomic-level simulations for $A\beta_{16-22}$ or any other sequence. Reviews of computational aggregation studies of amyloid peptides can be found in two recent articles.[28,29]

Calculations similar to those presented here, but without any cluster size analysis, have been reported earlier.[16] In that study no β-barrel was observed. The fact that we do so here could, in part, simply be due to improved statistics (by a factor 6). Another

Grant sponsor: Swedish Research Council.
*Correspondence to: A. Irbäck, Computational Biology and Biological Physics Group, Department of Theoretical Physics, Lund University, Sölvegatan 14A, SE-223 62 Lund, Sweden. E-mail: anders@thep.lu.se
Received 28 February 2007; Revised 7 May 2007; Accepted 23 May 2007
Published online 11 October 2007 in Wiley InterScience (www.interscience.wiley.com). DOI: 10.1002/prot.21682

difference is that we here use a slightly modified energy function that incorporates attractions and repulsions between side-chain charges (see Materials and Methods), which increase the stability of the β-barrel (see Results and Discussion).

MATERIALS AND METHODS

Model

The system we study consists of six $A\beta_{16-22}$ peptides (acetyl-Lys-Leu-Val-Phe-Phe-Ala-Glu-NH_2) contained in a periodic box of size $(50.4\ \text{Å})^3$, with implicit water. All atoms of the peptide chains are included in our calculations, but we assume fixed bond lengths, bond angles, and peptide torsion angles (180°), so that each residue only has the Ramachandran torsion angles ϕ, ψ and a number of side-chain torsion angles as its degrees of freedom. Numerical values of the geometrical parameters held constant can be found elsewhere.[30]

The energy function we use is a close variant of an energy function[30,31] that has been used to study the folding of several peptides with about 20 residues,[31] the aggregation of $A\beta_{16-22}$,[16] and the mechanical and thermal unfolding of ubiquitin.[32,33] It is composed of four terms,

$$E = E_{\text{loc}} + E_{\text{ev}} + E_{\text{hb}} + E_{\text{sc}}. \tag{1}$$

The term E_{loc} is an intrachain potential and is local in sequence. It represents an electrostatic interaction between adjacent peptide units along the chain. The other three terms are both intra- and interchain potentials and are nonlocal in sequence. The excluded volume term E_{ev} is a $1/r^{12}$ repulsion between pairs of atoms. E_{hb} represents two kinds of H bonds: backbone–backbone bonds and bonds between charged side chains and the backbone. The last term E_{sc} represents interactions between pairs of side chains. It is a simple pairwise additive potential based on the degree of contact between two side chains.

There is one major difference between the energy function used here and that used in the previous studies of this model.[16,31–33] The difference is in the term E_{sc}, which in the previous studies represented an effective hydrophobic attraction between pairs of nonpolar side chains. In the present study, we have incorporated attraction and repulsion between charged side chains into this term, while leaving the hydrophobicity part unchanged. The interaction between two charged side chains is assumed to be of short range because of screening by water, and is, for simplicity, taken to have the same functional form as the hydrophobic interaction between two nonpolar side chains.[31] Specifically, the new part is of the form

$$E_{\text{sc}}^{(q)} = \varepsilon_q \sum_{I<J} q_I q_J C_{IJ}, \tag{2}$$

where I and J denote charged residues, q_I and q_J are charges (± 1), and ε_q sets the strength of the interaction ($\approx$2.0 kcal/mol). C_{IJ} is a measure of the degree of contact between two amino acids

$$C_{IJ} = \frac{1}{N_I + N_J}\left[\sum_{i\in A_I} f(\min_{j\in A_J} r_{ij}^2) + \sum_{j\in A_J} f(\min_{i\in A_I} r_{ij}^2)\right]. \tag{3}$$

A_I denotes a predefined set of atoms: for Glu it is the two side-chain oxygens and for Lys the hydrogens in the NH_3-group (there are no Asp or Arg residues in $A\beta_{16-22}$). N_I and N_J are the number of atoms in the sets A_I and A_J. The function $f(x)$ is given by $f(x) = 1$ if $x < A$, $f(x) = 0$ if $x > B$, and $f(x) = (B - x)/(B - A)$ otherwise $[A = (3.5\ \text{Å})^2,\ B = (4.5\ \text{Å})^2]$. The form of the other energy terms has been described elsewhere.[31]

Having modified the energy function, we also recalibrated the energy scale of the model by folding simulations for the Trp cage peptide. The energy scale of the model is determined by using the model prediction for the melting temperature of Trp cage and the experimental value[34] for the same (315 K). On the internal scale of the model, the melting temperature changed by 2% (from 0.470 to 0.479) with the new energy function.

Simulation methods

The thermodynamics of aggregation for this system is investigated by using simulated tempering,[35–37] in which the temperature is a dynamical variable. This method is closely related to the replica exchange- or parallel tempering method.[38–40] The main difference is that simulated tempering works with only one copy of the system, whereas the replica exchange method simulates several copies of the system in parallel (which exchange temperatures with each other). Our simulations are carried out using the software package PROFASI.[41] A total of 30 independent simulated-tempering runs is collected. Ten of the runs span six temperatures from 293 to 362 K, whereas the other 20 runs span five temperatures from 306 K to 362 K. The six-temperature runs each comprise 10^{10} elementary MC steps. The length of each five-temperature run is 6×10^9 elementary MC steps. All the runs are started from random conformations.

For the backbone degrees of freedom, we use two different elementary moves: single-variable updates of individual torsion angles, which is a nonlocal method, and biased Gaussian steps,[42] a semilocal move that simultaneously updates up to eight angles. Side-chain angles are updated one by one. In addition to these updates, for computational efficiency, we also include rigid-body translations and rotations of whole chains. Every update

involves a Metropolis accept/reject step, thus ensuring detailed balance.

Measurements

To monitor the aggregation state of the system, we use a cluster-size analysis. Two chains I and J are said to be in the same cluster if the sum of their interchain side-chain interactions, $E_{sc}(I,J)$, and interchain backbone–backbone H bond energy, $E_{hb}^{bb}(I,J)$, is lower than a cutoff, $E_{sc}(I,J) + E_{hb}^{bb}(I,J) < -1.5\ \varepsilon_{hb}^{(1)}$, corresponding to 2–3 H bonds ($\varepsilon_{hb}^{(1)}$ sets the strength of backbone–backbone H bonds[31]). The cutoff is chosen to exclude brief random contacts, without being too restrictive. The size of the largest cluster in a given conformation is denoted by Λ. The clusters obtained by this definition are referred to as "general" clusters, or simply clusters, and may completely lack ordered secondary structure. We also use a stricter cluster definition. These clusters are referred to as "ordered" clusters. An ordered cluster is formed by pairs I, J of chains with $E_{hb}^{bb}(I,J) < -1.5\ \varepsilon_{hb}^{(1)}$ and a β-strand content, as defined below, higher than 0.3 for both chains. An ordered cluster is thus always part of a general cluster. The size of the largest ordered cluster is denoted by Λ_o.

For a chain with N amino acids, we define the α-helix and β-strand contents as the fractions of the $N - 2$ inner amino acids with their (ϕ,ψ) pair in the α-helix and β-strand regions of the Ramachandran space. We assume that α-helix corresponds to $-90^\circ < \phi < -30^\circ$, $-77^\circ < \psi < -17^\circ$ and that β-strand corresponds to $-150^\circ < \phi < -90^\circ$, $90^\circ < \psi < 150^\circ$. The average α-helix and β-strand contents, over all the chains of the system, are denoted by n_α and n_β, respectively.

To determine the amounts of parallel and antiparallel β-sheet structure in a given multichain conformation, we consider all possible pairs of chains. We first identify all chain pairs I, J such that their interchain backbone–backbone H bond energy satisfies $E_{hb}^{bb}(I,J) < -1.5\ \varepsilon_{hb}^{(1)}$, and both chains I and J have a β-strand content higher than 0.5. For each such pair of chains, we then calculate the scalar product of their normalized end-to-end unit vectors. If this scalar product is greater than 0.7 (less than -0.7), we say that the two chains are parallel (antiparallel). The number of parallel and antiparallel pairs of chains is denoted by n_+ and n_-, respectively.

The simulation data are analyzed using multihistogram techniques.[43] All statistical uncertainties quoted are 1σ errors obtained by the jackknife method.[44]

Figures of 3D structures were prepared using PyMOL.[45]*

β-Barrel geometry

The geometrical features of regular β-barrels are determined by the number of strands, n, and the shear number, S.[46–50] The shear number can be obtained by drawing a curve around the barrel perpendicular to the strands, from some reference strand until this strand is reached again. Let i and j be the residues on this strand at which the curve starts and ends, respectively. The shear number is $|i - j|$. In this definition, the curve can be traversed in either of two possible directions. If the direction is specified, the shear number can be given a sign. Because β-barrels have a right-handed twist, the sign is, however, not needed.

The tilt angle of the strands relative to the barrel axis, α, is given by $\tan\alpha = Sa/nb$, where the constants $a = 3.3$ Å and $b = 4.4$ Å are the C_α–C_α distances along the strands and the interstrand distance, respectively.

RESULTS AND DISCUSSION

Thermodynamics

Using the methods described earlier, we study the system of six $A\beta_{16-22}$ peptides in the temperature range 293 K $< T <$ 362 K. Figure 1(a) shows the calculated specific heat curve, which exhibits a sharp peak centered at $T = T_{max} \approx 335$ K. Our cluster size analysis (see Materials and Methods) reveals that large aggregated structures start to form around this temperature. Figure 1(b) shows the probability of having a cluster with five or six chains, $P(\Lambda \geq 5)$, against temperature. This probability increases from close to 0 at high temperature to more than 0.9 at low temperature, through a sigmoid-like transition centered in the vicinity of T_{max}. There is also a clear increase in β-strand content, $\langle n_\beta \rangle$, as the temperature decreases [see Fig. 1(c)]. The α-helix content, $\langle n_\alpha \rangle$, is, by contrast, small throughout the temperature range studied (data not shown). We thus find that the chains lack ordered secondary structure at high temperature, but form β-sheet structure at low temperature.

An interesting detail in Figure 1 is that $P(\Lambda \geq 5)$ starts to increase slightly before $\langle n_\beta \rangle$, as the temperature is decreased. At $T = T_{max}$, clusters with five or six chains occur with a significant frequency, whereas the β-strand content is small.

Figure 2(a) shows the probability that the largest cluster is of size n, $P(\Lambda = n)$, against temperature, for different n. The maximum of $P(\Lambda = 2)$ is at 357 K, which is well above the specific-heat maximum T_{max}. As n is increased, the maximum of $P(\Lambda = n)$ shifts toward lower temperature. Near T_{max}, all Λ are roughly equally probable, showing that clusters of all sizes occur. At low temperature, $\Lambda = 6$ is by far the most common value, so all the chains tend to form a single cluster.

Figure 2(b) shows an analysis similar to that in Figure 2(a) but for ordered clusters. Since an ordered cluster is always part of a general cluster, the size of the largest ordered cluster, Λ_o, cannot exceed Λ. Large ordered clusters are, in contrast to large general clusters, very rare at $T =$

*http://www.pymol.org/

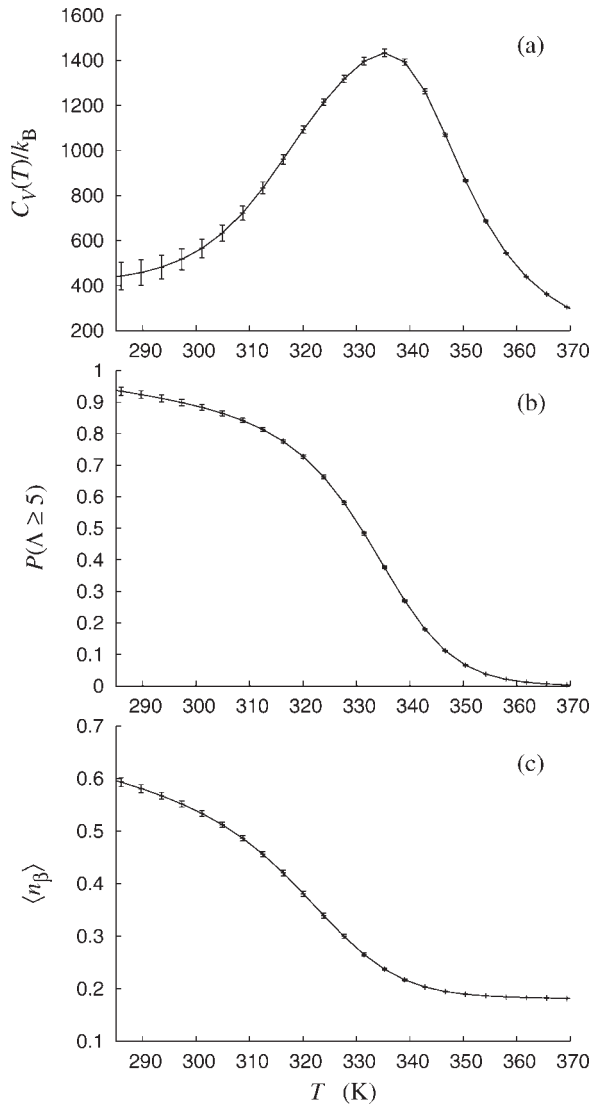

Figure 1

*Temperature dependence of (**a**) the specific heat $C_V = (\langle E^2 \rangle - \langle E \rangle^2)/k_B T^2$, (**b**) the probability that the size of the largest (general) cluster is 5 or 6, $P(\Lambda \geq 5)$, and (**c**) the β-strand content $\langle n_\beta \rangle$.*

T_{max}, where $P(\Lambda_o = 5)$ and $P(\Lambda_o = 6)$ both are close to 0. The absence of large ordered clusters is consistent with the finding that the β-strand content is small at $T = T_{max}$ [see Fig. 1(c)]. Large ordered clusters are, by contrast, common at the lowest temperatures studied, where $P(\Lambda_o \geq 5) > 0.5$.

The ordered aggregates seen at low temperature contain β-sheets, which can be either parallel, antiparallel, or mixed parallel/antiparallel. All these three kinds of β-sheet structure occur in our simulations. To find out whether there is a preference for parallel or antiparallel organization, we examine the probability distribution of the variables n_+ and n_- (see Materials and Methods), $P(n_+,n_-)$. Figure 3 shows $P(n,0)$ and $P(0,n)$ as functions of n at a fixed temperature of 306 K. $P(n,0)$ is markedly smaller than $P(0,n)$ for all n, implying that antiparallel structures are more common than parallel ones. For comparison, Figure 3 also shows the corresponding results from simulations with the interactions between side-chain charges switched off. As previously reported,[16] we find a clear preference for the antiparallel organization in this case too, although slightly weaker. This finding suggests that the interactions between side-chain charges alone are not responsible for the antiparallel organization seen in $A\beta_{16-22}$ experiments.[10–12]

Figure 4 shows the MC evolution of the energy E in two of our runs, along with some snapshots of long-lived aggregated structures. The simulation time is long enough for aggregated structures to both form and dissolve in the course of the runs, but simulating this system with >900 atoms is nevertheless a challenge. To test the convergence of our results, we computed the specific heat with statistical errors using two different data sets, the five- and six-temperature runs, respectively (see

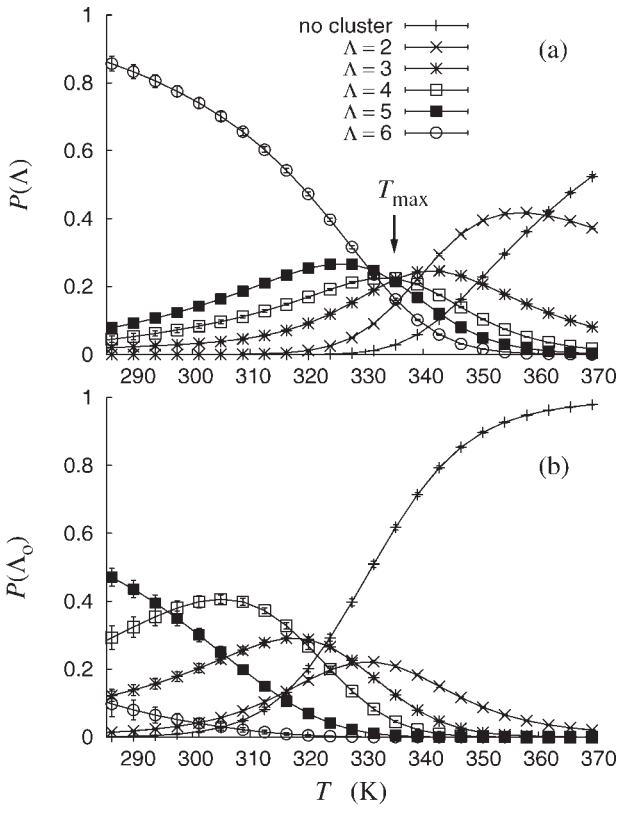

Figure 2

*(**a**) The probability that the largest general cluster is of size n, $P(\Lambda = n)$, against temperature, for n = 2,...,6. The curve labeled 'no cluster' is the probability that there is no cluster of size ≥2. The specific-heat maximum, T_{max}, is marked with an arrow. (**b**) The corresponding plot for ordered clusters.*

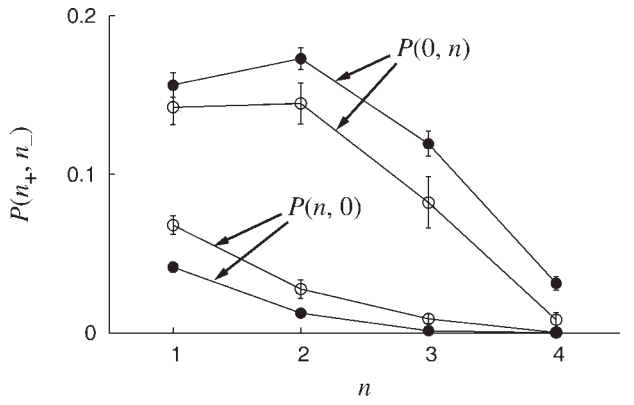

Figure 3

The probability distribution $P(n_+,n_-)$ for $(n_+,n_-) = (n,0)$ and $(n_+,n_-) = (0,n)$, against n, at 306 K, as obtained from simulations with (●) and without (○) interactions between charged side chains. The variables n_+ and n_- count parallel and antiparallel pairs of interacting β-strands (see Materials and Methods).

Materials and Methods). The results of the two analyses were in perfect agreement. This agreement suggests that the relative weights of high- and low-energy states are properly sampled, so that quantities like the specific heat can be reliably estimated.

Longer simulations would, by contrast, be needed in order to determine the relative weights of different low-energy states. Nevertheless, we next take a closer look at one particular low-energy state, the β-barrel. The β-barrel occurs in only one of our runs, the one shown in Figure 4(b), although several runs contain curved, almost closed β-sheets. The β-barrel has lower energy than any other observed state and stays intact over a very long period, about 5×10^9 MC steps [see Fig. 4(b)]. It is by far the most long-lived state seen in any of our simulations.

Another caveat of the analysis presented above is the small number of chains used. To make testable predictions for thermodynamic quantities like the temperature at which aggregation sets in, it would be necessary to study larger systems. New techniques for encapsulating peptides are, however, being developed,[51] which have the potential to facilitate future comparisons of experimental and computational studies.

Structure and stability of the β-barrel

The geometry of regular β-barrel structures can be classified by the number of strands, n, and the shear number, S (see Materials and Methods).[46–50] It has been argued that regular β-barrels with good β-sheet geometries and well-packed interiors can be obtained only for a limited set of 10 different (n,S) pairs, namely $(n,8)$ with $4 \leq n \leq 8$, $(n,10)$ with $5 \leq n \leq 8$, and with $(n,S) = (6,12)$.[48,49] For $n = 6$, the preferred values of S are 8, 10, and 12. The corresponding tilt angles are in the range 45°–56°.

Figure 5 shows a schematic snapshot of the β-barrel observed in our simulations. It is (right-) twisted, as it should, and composed of six antiparallel strands that are tilted relative to the barrel axis. A closer inspection reveals that among the six pairs of adjacent strands, the alignment is in register for one pair and out of register by two residue units for the other five pairs, leading to a shear number of $S = 10$. The observed barrel thus has one of the three preferred S values for regular six-stranded barrels. In fact, $S = 10$ is expected to be optimal with respect to β-sheet geometry, given $n = 6$.[48] The (n,S) classification of this barrel is thus perfectly consistent with its high apparent stability [see Fig. 4(b)].

At first glance, a β-barrel may seem inconsistent with IR experiments on $A\beta_{16-22}$ in solution,[12] which found evidence for an antiparallel in-register β-sheet structure, corresponding to $S = 0$. However, this behavior was observed after a relaxation period, during which the

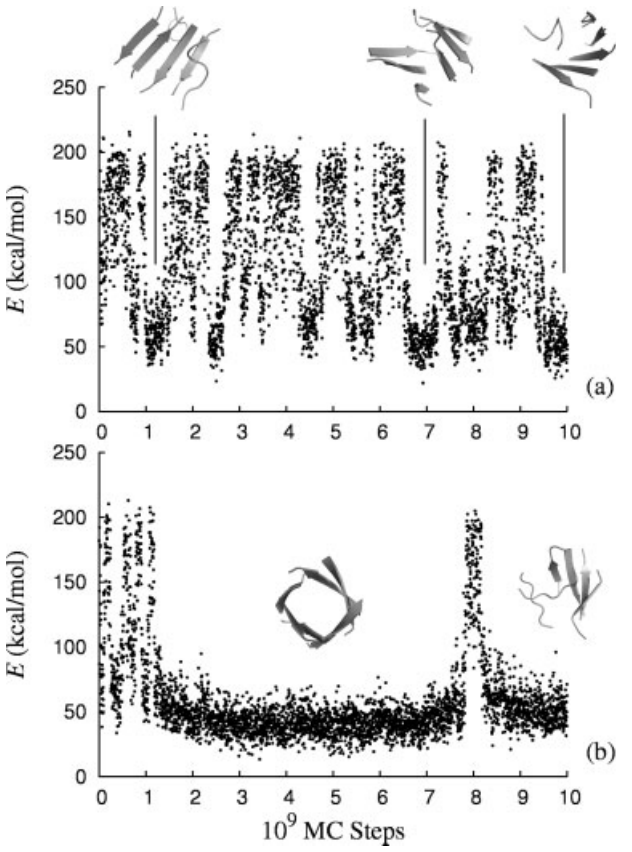

Figure 4

MC evolution of the energy in two simulated-tempering runs for the system of six $A\beta_{16-22}$ peptides. Also shown are some snapshots of long-lived aggregates that formed in the course of the runs.

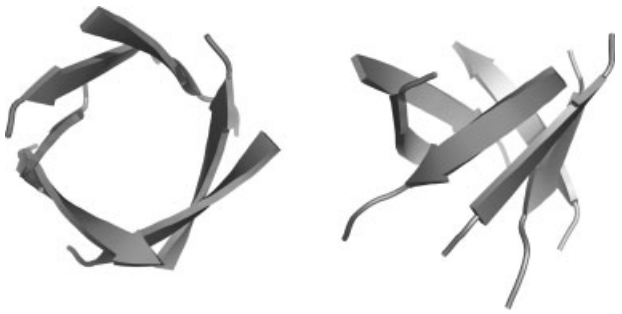

Figure 5

Schematic snapshot of the β-barrel that formed in one of our runs. The two pictures are different views of the same structure.

spectra changed with time. A nonnegligible β-barrel population might have been present in the early stages.

Our calculations aim at exploring thermodynamically relevant states of the system, rather than the kinetics of the aggregation process. Nevertheless, they can elucidate possible pathways for the formation of $A\beta_{16-22}$ oligomers. Figure 6 illustrates how the configuration of ordered clusters evolves with MC time in two runs. The first run [Fig. 6(a)] is the one containing the β-barrel. The barrel is present over a period extending roughly from 2×10^9 MC steps to 7×10^9 MC steps, during which the chains tend to form an ordered cluster of size 6. Immediately before the formation of the barrel, there is a brief phase in which the largest ordered cluster is typically of size 5. This period is, in turn, preceded by a stage dominated by '3 + 3' conformations, which have two ordered clusters of size 3. During the whole duration of the intermediate peak for ordered clusters of size 5, it turns out that the probability of having a general cluster of size 6 is above 0.8 (data not shown). So, all chains are in contact most of this time, but one chain forms less ordered contacts with the other chains. The emerging picture is that of two three-stranded β-sheets merging to form the barrel, although it is not a simple docking of two rigid structures.

An ordered cluster of size 6 occurs in the second run as well [Fig. 6(b)]. It is present approximately between 1.0×10^9 MC steps and 1.8×10^9 MC steps. Inspection of snapshots from the run shows that this cluster corresponds to a six-stranded β-sheet that is curved but not closed. The formation of this state occurs through addition of chains one by one to a growing β-sheet, rather than through fusion of two smaller β-sheets. Growth by monomer addition has been experimentally verified as a viable mechanism of fibril formation.[52]

The $A\beta_{16-22}$ peptide has two charged side chains, which are those of the end residues Lys16 and Glu22. The formation of the β-barrel, with antiparallel strands, brings oppositely charged side chains close to each other. The interactions between these charges might be crucial for the stability of the β-barrel, especially since the number of chains is even, so that a closed structure can be created without getting any conflicting pair of nearby like charges. To test the importance of the interactions between side-chain charges, we study the stability of the β-barrel both with and without these interactions in the model. For each of the two cases, 100 runs are performed at a constant temperature of 334 K, which is near the

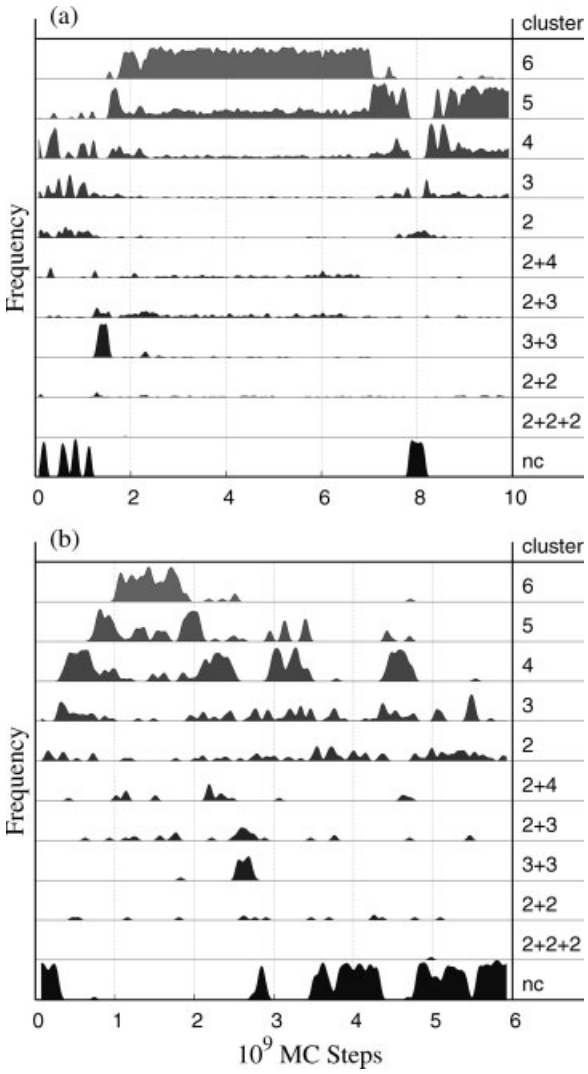

Figure 6

*The probability of different configurations of ordered clusters against MC time in two simulated-tempering runs. A label 'n' stands for conformations with one ordered cluster of size n, 'n + m' for conformations with two ordered clusters of sizes n and m, etc., whereas 'nc' denotes conformations without any ordered cluster. The probabilities are calculated as sliding averages over the respective time series, using a Gaussian weight factor with a variance of 3×10^7 MC steps. (**a**) The run in which a β-barrel formed [same as in Figure 4(b)]. (**b**) A run in which a curved but not closed six-stranded β-sheet occurs.*

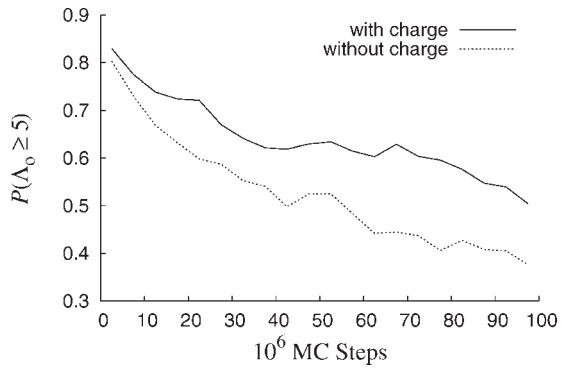

Figure 7

MC evolution of the probability of having an ordered cluster of size ($\Lambda_o \geq 5$) at 334 K, in runs with the β-barrel in Figure 5 as the initial conformation. The two curves represent simulations with (solid) and without (dashed) interactions between charged side chains, respectively. To reduce noise, raw data are binned into subintervals of size 5×10^6 MC steps. Each curve is an average over 100 runs.

specific-heat maximum T_{max}. In these stability tests, we do not use the nonlocal single-variable update of backbone angles (see Materials and Methods). The runs are started with the β-barrel as the initial conformation. Figure 7 shows the MC evolution of the probability of having an ordered cluster of size 5 or 6, $P(\Lambda_o \geq 5)$, as obtained from these two sets of runs. Initially, this probability is 1, since $\Lambda_o = 6$ for the β-barrel conformation. The subsequent decay of $P(\Lambda_o \geq 5)$ is seen to be faster if the interactions between side-chain charges are removed from the model, which shows that the β-barrel indeed is less stable in this case. The difference is, however, quantitative rather than qualitative. The β-barrel remains a local free-energy minimum, although less pronounced, in the absence of these interactions.

CONCLUSION

To explore the nature of small oligomers of the fibril-forming $A\beta_{16-22}$ peptide, we have performed an all-atom study of six $A\beta_{16-22}$ peptides enclosed in a periodic box. A simple but useful cluster-size analysis was devised and employed to characterize multichain conformations with respect to aggregates. The analysis distinguishes between general and ordered clusters. At the onset of aggregation, where the specific heat has a sharp peak, general clusters of all sizes were found to occur. Large ordered clusters are, by contrast, rare at this temperature. This difference indicates that hydrophobic association tends to precede secondary-structure formation in the aggregation process. The formation of ordered aggregates may involve fusion of two smaller aggregates, or occur by monomer addition to a growing β-sheet. The runs discussed in Figure 6, although not kinetic simulations, illustrate these two types of behavior.

At low temperature, the aggregated structures were found to be β-sheet rich, with either parallel, antiparallel, or mixed parallel/antiparallel strands. While all these three possibilities occur in the simulations, a clear statistical preference was found for antiparallel over parallel alignment, which is consistent with $A\beta_{16-22}$ experiments.[10–12] It is worth noting that the antiparallel preference persists, though slightly reduced, upon removal of the interactions between side-chain charges. This finding suggests that these interactions are not alone responsible for the antiparallel alignment, but other factors play a significant role, too.

In one of our runs, the six chains spontaneously self-assembled into a β-barrel. It occurred only once in 30 runs, but once formed, the β-barrel remained intact over an extraordinary long period, about 5×10^9 MC steps. This behavior suggests that the β-barrel represents a sharp but not easily accessible minimum on the free-energy landscape. Many other aggregated conformations were also seen in the simulations, indicating a rugged free-energy landscape with many distinct minima.

The observed β-barrel has six antiparallel strands and a shear number of $S = 10$. This value of S is what one expects for a six-stranded barrel with optimal β-sheet geometry,[48] which in part explains the high apparent stability of the state.

For peptides in the diverse class of amyloid-forming sequences, the β-barrel motif is a natural but not obvious candidate for a relatively stable oligomeric state. A β-barrel, indeed, is the most long-lived species found in our $A\beta_{16-22}$ simulations. To address the question of whether the ability to form β-barrels is a common property among amyloid-forming peptides, it would be interesting to extend these calculations to other sequences.

ACKNOWLEDGMENTS

The authors thank Sandipan Mohanty for valuable discussions. The simulations were performed at the LUNARC facility at Lund University.

REFERENCES

1. Lansbury PT, Jr, Lashuel HA. A century-old debate on protein aggregation and neurodegeneration enters the clinic. Nature 2006; 443:774–779.
2. Teplow DB, Lazo ND, Bitan G, Bernstein S, Wyttenbach T, Bowers MT, Baumketner A, Shea JE, Urbanc B, Cruz L, Borreguero J, Stanley HE. Elucidating amyloid β-protein folding and asembly: a multidisciplinary approach. Acc Chem Res 2006;39:635–645.
3. Lesné S, Koh MT, Kotilinek L, Kayed R, Glabe CG, Yang A, Gallagher M, Ashe KH. A specific amyloid-β protein assembly in the brain impairs memory. Nature 2006;440:352–356.
4. Jaroniec CP, MacPhee CE, Bajaj VS, McMahon MT, Dobson CM, Griffin RG. High-resolution molecular structure of a peptide in an

amyloid fibril determined by magic angle spinning NMR spectroscopy. Proc Natl Acad Sci USA 2004;101:711–716.
5. Luehrs T, Ritter C, Adrian M, Riek-Loher D, Bohrmann B, Döbeli H, Schubert D, Riek R. 3D structure of Alzheimers amyloid-(1-42) fibrils. Proc Natl Acad Sci USA 2005;102:17342–17347.
6. Nelson R, Sawaya MR, Balbirnie M, Madsen AØ, Riekel C, Grothe R, Eisenberg D. Structure of the cross-β spine of amyloid-like fibrils. Nature 2005;435:773–778.
7. Makin OS, Atkins E, Sikorski P, Johansson J, Serpell LC. Molecular basis for amyloid fibril formation and stability. Proc Natl Acad Sci USA 2005;102:315–320.
8. Lashuel HA, Lansbury PT, Jr. Are amyloid diseases caused by protein aggregates that mimic bacterial pore-forming toxins? Q Rev Biophys 2006;39:167–201.
9. Arispe N, Pollard HB, Rojas E. Beta-amyloid Ca^{2+}-channel hypothesis for neuronal death in Alzheimer disease. Mol Cell Biochem 1994;140:119–125.
10. Balbach JJ, Ishii Y, Antzutkin ON, Leapman RD, Rizzo NW, Dyda F, Reed J, Tycko R. Amyloid fibril formation by $A\beta_{16-22}$, a seven-residue fragment of the Alzheimer's β-amyloid peptide, and structural characterization by solid state NMR. Biochemistry 2000;39:13748–13759.
11. Gordon DJ, Balbach JJ, Tycko R, Meredith SC. Increasing the amphiphilicity of an amyloidogenic peptide changes the β-sheet structure in the fibrils from antiparallel to parallel. Biophys J 2004;86:428–434.
12. Petty SA, Decatur SM. Experimental evidence for the reorganization of β-strands within aggregates of the $A\beta_{16-22}$ peptide. J Am Chem Soc 2005;127:13488–13489.
13. Tjernberg LO, Näslund J, Lindqvist F, Johansson J, Karlström AR, Thyberg J, Terenius L, Nordstedt C. Arrest of β-amyloid fibril formation by pentapeptide ligand. J Biol Chem 1996;271:8545–8548.
14. Ma B, Nussinov R. Stabilities and conformations of Alzheimer's β-amyloid peptide oligomers ($A\beta_{16-22}$, $A\beta_{16-35}$, and $A\beta_{10-35}$): sequence effects. Proc Natl Acad Sci USA 2002;99:14126–14131.
15. Klimov DK, Thirumalai D. Dissecting the assembly of $A\beta_{16-22}$ amyloid peptides into antiparallel β sheets. Structure 2003;11:295–307.
16. Favrin G, Irbäck A, Mohanty S. Oligomerization of amyloid $A\beta_{16-22}$ peptides using hydrogen bonds and hydrophobicity forces. Biophys J 2004;87:3657–3664.
17. Santini S, Mousseau N, Derreumaux P. In silico assembly of Alzheimer's $A\beta_{16-22}$ peptide into β-sheets. J Am Chem Soc 2004;126:11509–11516.
18. Hwang W, Zhang S, Kamm RD, Karplus M. Kinetic control of dimer structure formation in amyloid fibrillogenesis. Proc Natl Acad Sci USA 2004;101:12916–12921.
19. Klimov DK, Straub JE, Thirumalai D. Aqeous urea solution destabilizes $A\beta_{16-22}$ oligomers. Proc Natl Acad Sci USA 2004;101:14760–14765.
20. Röhrig UF, Laio A, Tantalo N, Parrinello M, Petronzio R. Stability and structure of oligomers of the Alzheimer peptide $A\beta_{16-22}$: from the dimer to the 32-mer. Biophys J 2006;91:3217–3229.
21. Meinke JH, Hansmann UHE. Aggregation of β-amyloid fragments. J Chem Phys 2007;126:014706.
22. Nguyen PH, Li MS, Stock G, Straub JE, Thirumalai D. Monomer adds to preformed structured oligomers of Aβ-peptides by a two-stage dock-lock mechanism. Proc Natl Acad Sci USA 2007;104:111–116.
23. Gnanakaran S, Nussinov R, García AE. Atomic-level description of amyloid β-dimer formation. J Am Chem Soc 2006;128:2158–2159.
24. Friedel M; Shea JE. Self-assembly of peptides into a β-barrel motif. J Chem Phys 2004;120:5809–5823.
25. Marchut AJ, Hall CK. Spontaneous formation of annular structures observed in molecular dynamics simulations of polyglutamine peptides. Comput Biol Chem 2006;30:215–218.
26. Wei G, Mousseau N, Derreumaux P. Sampling the self-assembly pathways of KFFE hexamers. Biophys J 2004;87:3648–3656.
27. Melquiond A, Mousseau N, Derreumaux P. Structures of soluble amyloid oligomers from computer simulations. Proteins 2006;65:180–191.
28. Ma B, Nussinov R. Simulations as analytical tools to understand protein aggregation and predict amyloid formation. Curr Opin Chem Biol 2006;10:1–8.
29. Gsponer J, Vendruscolo M. Theoretical approaches to protein aggregation. Protein Pept Lett 2006;13:287–293.
30. Irbäck A, Samuelsson B, Sjunnesson F, Wallin S. Thermodynamics of α- and β-structure formation in proteins. Biophys J 2003;85:1466–1473.
31. Irbäck A, Mohanty S. Folding thermodynamics of peptides. Biophys J 2005;88:1560–1569.
32. Irbäck A, Mitternacht S, Mohanty S. Dissecting the mechanical unfolding of ubiquitin. Proc Natl Acad Sci USA 2005;102:13427–13432.
33. Irbäck A, Mitternacht S. Thermal versus mechanical unfolding of ubiquitin. Proteins 2006;65:759–766.
34. Neidigh JW, Fesinmeyer RM, Andersen NH. Desiging a 20-residue protein. Nat Struct Biol 2002;9:425–430.
35. Lyubartsev AP, Martsinovski AA, Shevkunov SV, Vorontsov-Velyaminov PN. New approach to Monte Carlo calculation of the free energy: method of expanded ensembles. J Chem Phys 1992;96:1776–1783.
36. Marinari E, Parisi G. Simulated tempering: a new Monte Carlo scheme. Europhys Lett 1992;19:451–458.
37. Irbäck A, Potthast F. Studies of an off-lattice model for protein folding: sequence dependence and improved sampling at finite temperature. J Chem Phys 1995;103:10298–10305.
38. Tesi MC, van Rensburg EJJ, Orlandini E, Whittington SG. Monte Carlo study of the interacting self-avoiding walk model in three dimensions. J Stat Phys 1996;82:155–181.
39. Hukushima K, Nemoto K. Exchange Monte Carlo method and application to spin glass simulations. J Phys Soc Jpn 1996;65:1604–1608.
40. Hansmann UHE. Parallel tempering algorithm for conformational studies of biological molecules. Chem Phys Lett 1997;281:140–150.
41. Irbäck A, Mohanty S. PROFASI: a Monte Carlo simulation package for protein folding and aggregation. J Comput Chem 2006;27:1548–1555.
42. Favrin G, Irbäck A, Sjunnesson F. Monte Carlo update for chain molecules: biased Gaussian steps in torsional space. J Chem Phys 2001;114:8154–8158.
43. Ferrenberg AM, Swendsen RH. Optimized Monte Carlo data analysis. Phys Rev Lett 1989;63:1195–1198.
44. Miller, R.G. The jackknife—a review. Biometrika 1974;61:1–15.
45. DeLano WL. The PyMOL molecular graphics system. San Carlos, CA: DeLano Scientific; 2002.
46. McLachlan AD. Gene duplication in the structural evolution of chymotrypsin. J Mol Biol 1979;128:49–79.
47. Chou KC, Carlacci L, Maggiora GG. Conformational and geometrical properties of idealized β-barrels in proteins. J Mol Biol 1990;168:389–407.
48. Murzin AG, Lesk AM, Chothia C. Principles determining the structure of β-sheet barrels in proteins. I. A theoretical analysis. J Mol Biol 1994;236:1369–1381.
49. Murzin AG, Lesk AM, Chothia C. Principles determining the structure of β-sheet barrels in proteins. II. The observed structures. J Mol Biol 1994;236:1382–1400.
50. Liu WM. Shear numbers of protein β-barrels: definition refinements and statistics. J Mol Biol 1998;275:541–545.
51. Lazar KL, Kurutz JW, Tycko R, Meredith SC. Encapsulation and NMR on an aggregating peptide before fibrillogenesis. J Am Chem Soc 2006;128:16460–16461.
52. Collins SR, Douglas A, Vale RD, Weissman JS. Mechanism of prion propagation: amyloid growth occurs by monomer addition. PLoS Biol 2004;2:1582–1590.